nature communications

Article

https://doi.org/10.1038/s41467-024-52953-8

The gut microbiome is associated with susceptibility to febrile malaria in Malian children

Received: 22 March 2024

Accepted: 23 September 2024

Published online: 05 November 2024

Check for updates

Kristin M. Van Den Ham[1], Layne K. Bower[1], Shanping Li[2], Hernan Lorenzi[3], Safiatou Doumbo[4], Didier Doumtabe[4], Kassoum Kayentao[4], Aissata Ongoiba[4], Boubacar Traore[4], Peter D. Crompton[2] & Nathan W. Schmidt[1]

Malaria is a major public health problem, but many of the factors underlying the pathogenesis of this disease are not well understood, including protection from the development of febrile symptoms, which is observed in individuals residing in areas with moderate-to-high transmission by early adolescence. Here, we demonstrate that susceptibility to febrile malaria following *Plasmodium falciparum* infection is associated with the composition of the gut microbiome prior to the malaria season in 10-year-old Malian children, but not in younger children. Gnotobiotic mice colonized with the fecal samples of malaria-susceptible children were shown to have a significantly higher parasite burden following *Plasmodium* infection compared to gnotobiotic mice colonized with the fecal samples of malaria-resistant children. The fecal microbiome of the susceptible children was determined to be enriched for bacteria associated with inflammation, mucin degradation and gut permeability, and to have increased levels of nitric oxide-derived DNA adducts and lower levels of mucus phospholipids compared to the resistant children. Overall, these results indicate that the composition of the gut microbiome is associated with the prospective risk of febrile malaria in Malian children and suggest that modulation of the gut microbiome could decrease malaria morbidity in endemic areas.

Plasmodium falciparum infection remains a major cause of morbidity and mortality in tropical and subtropical regions throughout the world. There were 249 million cases and 608,000 deaths due to malaria in 2022, the majority of which occurred in children in the World Health Organization African region[1]. The clinical manifestation of *P. falciparum* infection can range from asymptomatic to severe and fatal symptoms, including respiratory distress and cerebral malaria. The proportion of *P. falciparum* infections that are asymptomatic is known to increase as the transmission intensity and the prevalence of malaria in the community increases[2]. Moreover, individuals residing in areas with moderate-to-high levels of transmission typically develop protection from severe symptoms in early childhood and protection from febrile symptoms by early adolescence[3–5]. However, the factors responsible for modulating malaria pathogenesis have not been fully defined.

The gut microbiome is increasingly recognized as playing a role in the etiology of numerous diseases[6–8], including those caused by

[1]Ryan White Center for Pediatric Infectious Diseases and Global Health, Herman B Wells Center for Pediatric Research, Department of Pediatrics, Indiana University School of Medicine, Indianapolis, IN, USA. [2]Malaria Infection Biology and Immunity Section, Laboratory of Immunogenetics, National Institute of Allergy and Infectious Diseases, National Institutes of Health, Rockville, MD, USA. [3]Infectious Diseases Group, J. Craig Venter Institute, Bethesda, MD, USA. [4]Mali International Center of Excellence in Research; Malaria Research and Training Center, University of Sciences, Techniques and Technologies of Bamako, Bamako, Mali. e-mail: nwschmid@iu.edu

intestinal and extraintestinal pathogens[9–11]. The susceptibility of mice to *Plasmodium* infection, as measured by their parasite burden, has been established to be highly dependent on the composition of their gut microbiome[10,12], but the influence of the gut microbiome on clinical malaria outcomes in humans is less well characterized. In a cross-sectional study, the composition of the fecal microbiome was shown to be different between Ugandan infants (aged 0.5–4 years) with severe malarial anemia and those with asymptomatic *P. falciparum* infection[12,13], but whether the differences in the microbiome engendered the differences in malaria severity or were the result of the differential severity is unclear. Additionally, a longitudinal study in a cohort of Malian children and adults (aged 0.25–25 years) found that the fecal microbiome composition before the start of the malaria season correlated with the prospective risk of *P. falciparum* infection, but not with the development of febrile malaria[14]. Since the risk of developing febrile malaria decreases with age/malaria exposure in endemic areas and the gut microbiome also varies with age[15], it is possible that the wide age range of participants in this study left it underpowered to detect age-specific correlations between the microbiome and the risk of febrile malaria.

Here, we demonstrate that the fecal microbiome before the start of the malaria transmission season correlates with susceptibility to the development of febrile malaria following *P. falciparum* infection during the ensuing malaria season in 10-year-old Malian children, but not in younger children. Gnotobiotic mice colonized with fecal samples collected from malaria-susceptible children had a significantly higher parasite burden following *Plasmodium* infection than those colonized with fecal samples from malaria-resistant children. Susceptibility to febrile malaria correlated with a higher abundance of bacteria that have previously been associated with inflammatory bowel disease (IBD), intestinal mucus barrier degradation, and inflammation, but also with bacteria that have been associated with remission following dysbiotic intestinal events. Metabolomics validated the potential metabolic activity indicated by the shotgun metagenomics analysis, with the fecal samples of the susceptible children having increased levels of both metabolites associated with nitric oxide-induced inflammatory damage and impaired barrier function and metabolites associated with recovery following intestinal dysbiosis. The results of this longitudinal study demonstrate that differences in the gut microbiome are associated with differences in the prospective risk of febrile malaria symptoms in Malian children. Further investigation into these differences has the potential to lead to interventions that limit malaria morbidity.

Results

Classification of Malian children as resistant or susceptible to febrile malaria

The study was conducted in Kalifabougou, Mali, where *P. falciparum* transmission is seasonal; the majority of infections occur between July and December each year[16]. Children aged 6 to 10 years old ($n = 181$) were enrolled in a prospective cohort study from May 2014 to March 2015. Fecal samples from 156 of the children were included in the microbiome analysis after removing children who were missing fecal samples ($n = 2$) or who did not have a detected *P. falciparum* infection (by PCR or microscopy) during the study period ($n = 23$) (Supplementary Data 1).

We were interested in determining if the gut microbiome of these children was associated with the clinical outcome of *P. falciparum* infection. Children were initially characterized as susceptible if they experienced at least one febrile malaria episode during the study period and as resistant if they had no febrile malaria episodes during the study period despite having at least one asymptomatic *P. falciparum* detected by PCR. Asymptomatic *P. falciparum* infections were detected at monthly scheduled visits, while febrile malaria episodes were detected at the same scheduled visits and during unscheduled sick visits. Almost all of the children under 10 years of age were susceptible to febrile malaria (83 out of 86 children), whereas a quarter of the 10-year-old children were resistant to the development of febrile symptoms following infection (16 out of 70 children) (Supplementary Data 1).

Susceptibility to febrile malaria corresponds with the gut microbiome composition in 10-year-old children

Transmission of *P. falciparum* in Mali is seasonal, thus the dry season (January to May) offers an approximate wash-out period between successive transmission seasons. Consequently, we analyzed the fecal samples collected in May to determine if the microbiome composition prior to the start of the transmission season prospectively correlated with the risk of febrile malaria during the ensuing season. Since the gut microbiome varies with age[15] and individuals residing in areas with moderate-to-high levels of *Plasmodium* transmission typically develop protection from febrile symptoms by early adolescence[3–5], we hypothesized that this protection might be, at least in part, related to age-dependent changes in the microbiome. The microbiome composition was found to be significantly different between the malaria-resistant and the malaria-susceptible 10-year-old children (PERMANOVA; $P = 0.030$) using Bray-Curtis dissimilarity (Fig. 1A), but was also different not only between the children under the age of 10 and the 10-year-old children (PERMANOVA; $P = 0.0470$) but also between the susceptible children under the age of 10 and the susceptible 10-year-old children (PERMANOVA; $P = 0.0465$). These results suggest that the protection that develops against febrile symptoms by early adolescence may be related to age-dependent microbiome changes and that if the microbiome plays a role in determining malaria susceptibility in younger children, it is likely dependent on different microbiome composition differences than those present in the 10-year-old children.

Parasite burden of the humanized gnotobiotic mice corresponds with the susceptibility of the human donor to febrile malaria

A humanized gnotobiotic mouse model was employed to determine if there was a causal link between the gut microbiome of the Malian children and malaria susceptibility. Fecal samples were chosen to cover the space spanned by the principal components (Fig. 1A). Four susceptible children (subject IDs 375, 400, 415, and 446) and four resistant children (subject IDs 404, 417, 450, and 452) were selected, and the May fecal sample from each child was used to colonize four sex-matched germ-free mice (GF). The colonized mice were then infected with *Plasmodium yoelii* and parasitemia was followed until the infection cleared.

Overall, the mice that were colonized with the fecal samples from the resistant children had significantly lower parasitemia ($P = 0.0136$) than the mice that were colonized with the fecal samples from the susceptible children (Fig. 1B, C). One mouse colonized with the fecal sample of resistant donor 404 and one mouse colonized with the fecal sample of resistant donor 452 developed high parasitemia (Fig. 1D). This phenomenon has also been observed in mice that are known to possess a microbiome associated with a low level of parasitemia (Tac)[10] (Supp. Fig. 1A, B), as well as in true GF, which typically have low levels of parasitemia following infection with *P. yoelii* (Supp. Fig. 1A, B), suggesting an additional non-microbiome-associated source of variation in the parasitemia.

Mice colonized with the fecal sample of susceptible donor 415 exhibited low parasitemia. Given this outlier, we more closely examined the incidence of asymptomatic *P. falciparum* infections and febrile malaria episodes in the four susceptible donors. Over the study period, susceptible subjects 375, 400, and 446 each experienced 3–4 febrile malaria episodes while no asymptomatic infections were detected (Supplementary Data 2), consistent with their malaria-

https://doi.org/10.1038/s41467-024-52953-8

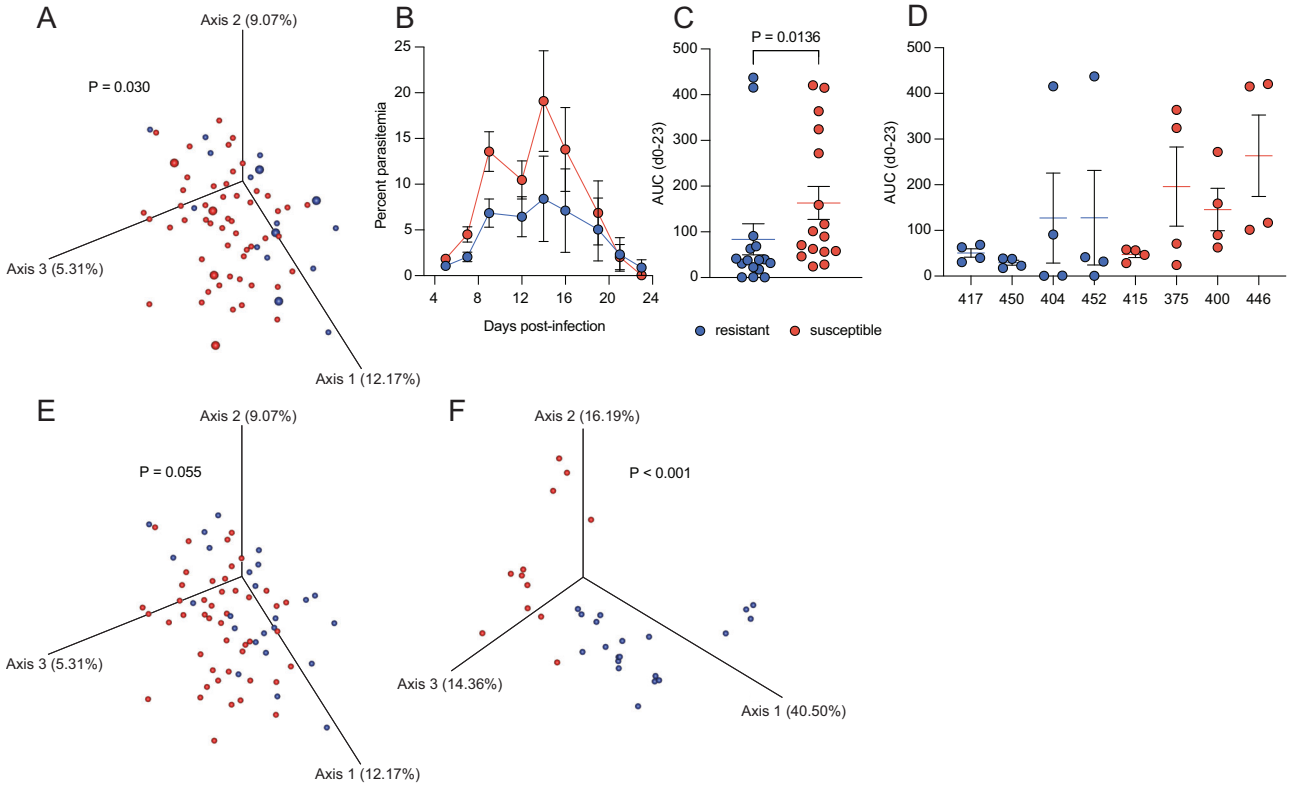

Fig. 1 | Microbiome composition correlates with susceptibility to febrile malaria in children and high parasite burden in mice. A Principal coordinate analysis (PCoA) plot of the Bray-Curtis dissimilarity of the human fecal samples using 16S rRNA sequencing. Gavage samples are highlighted by increased point size. **B** Parasitemia and **C** AUC of the gavaged gnotobiotic mice by resistant and susceptible outcome groups, and **D** parasitemia by individual gavage groups. $n = 4$ mice for each donor used. $n = 16$ for the overall resistant and susceptible groups. PCoA plots of the Bray-Curtis dissimilarity for the **E** human and the **F** murine fecal samples using 16S rRNA sequencing and the updated resistant definition. The P value for the Bray–Curtis distance was determined using a two-sided PERMANOVA, and the P value for the parasitemia was determined using a two-sided Mann–Whitney U test. Blue circles indicate resistant children or low parasitemia mice, and red circles indicate susceptible children or high parasitemia mice. Mean ± standard error of the mean (SEM) indicated for parasitemia and AUC.

susceptible phenotype. In contrast, subject 415 experienced two febrile malaria episodes and was asymptomatically infected at five timepoints (Supplementary Data 2), indicating a higher degree of malaria resistance.

A similar analysis of the cumulative incidence of asymptomatic *P. falciparum* infections and febrile malaria episodes among all 70 10-year-old children showed that 26 children initially classified as malaria-susceptible had both asymptomatic and febrile infections, eight of which had 1 to 2 febrile malaria episodes and were asymptomatically infected at five or more timepoints during the study period (Supplementary Data 2). Re-analysis of the 16S rRNA sequencing after reclassifying these eight children as malaria-resistant showed a similar trend to that which was observed using the initial definition of malaria resistance and susceptibility ($P = 0.055$) (Fig. 1E).

16S rRNA sequencing was performed on the fecal samples collected from the mice on the day of infection, and the engrafted microbiomes were determined to be significantly different ($P < 0.001$) between the groups of mice colonized with fecal samples from malaria-resistant children versus malaria-susceptible children using Bray–Curtis dissimilarity (Fig. 1F).

Differential parasite burden in mice is primarily associated with Eubacteriales species

Differential abundance analysis was performed on the mouse 16S rRNA sequencing data to examine the relationship between the microbiome and parasite burden (Supplementary Data 3). *Eubacterium coprostanoligenes*, *Gemmiger formicilis*, *Anaerostipes hadrus,* and *Roseburia faecis* were significantly increased in the low parasitemia mouse groups (Fig. 2A–D). *Clostridium citroniae*, *Dorea longicatena*, *Coprococcus comes*, *Blautia faecis*, *Bacteroides intestinalis*, and *Bacteroides ovatus*, as well as two unclassified species, *Clostridium* sp. FS41, *Ruminococcus* sp. Marseille-P328, were significantly increased in the high parasitemia mouse groups (Fig. 2E–L). Interestingly, many of the bacteria that were significantly more abundant in the high parasite burden mice have previously been shown to be associated with impaired gut barrier function and to be enriched during IBD[17–19].

Resistance to febrile malaria is associated with *Streptococcus thermophilus* and susceptibility with *Ruminococcus, Dorea,* and *Blautia* species

Differential abundance analysis was performed on the human 16S rRNA sequencing data to further investigate the association of the microbiome with susceptibility (Supplementary Data 4). *Streptococcus thermophilus* was significantly more abundant in the microbiome of the resistant children (Fig. 2M), and unclassified species of *Ruminococcus*, *Dorea*, and *Blautia* were significantly more abundant in the susceptible children (Fig. 2N–P).

Discrimination of malaria-resistant and -susceptible children improved by increased sequencing depth

Since we demonstrated that the microbiome is causally linked to malaria susceptibility using a gnotobiotic mouse model, we performed shotgun metagenomics sequencing on the human samples to better understand the microbiome composition and the interactions underlying susceptibility to febrile malaria through the increased sequencing depth and the improved classification at the species level afforded

https://doi.org/10.1038/s41467-024-52953-8

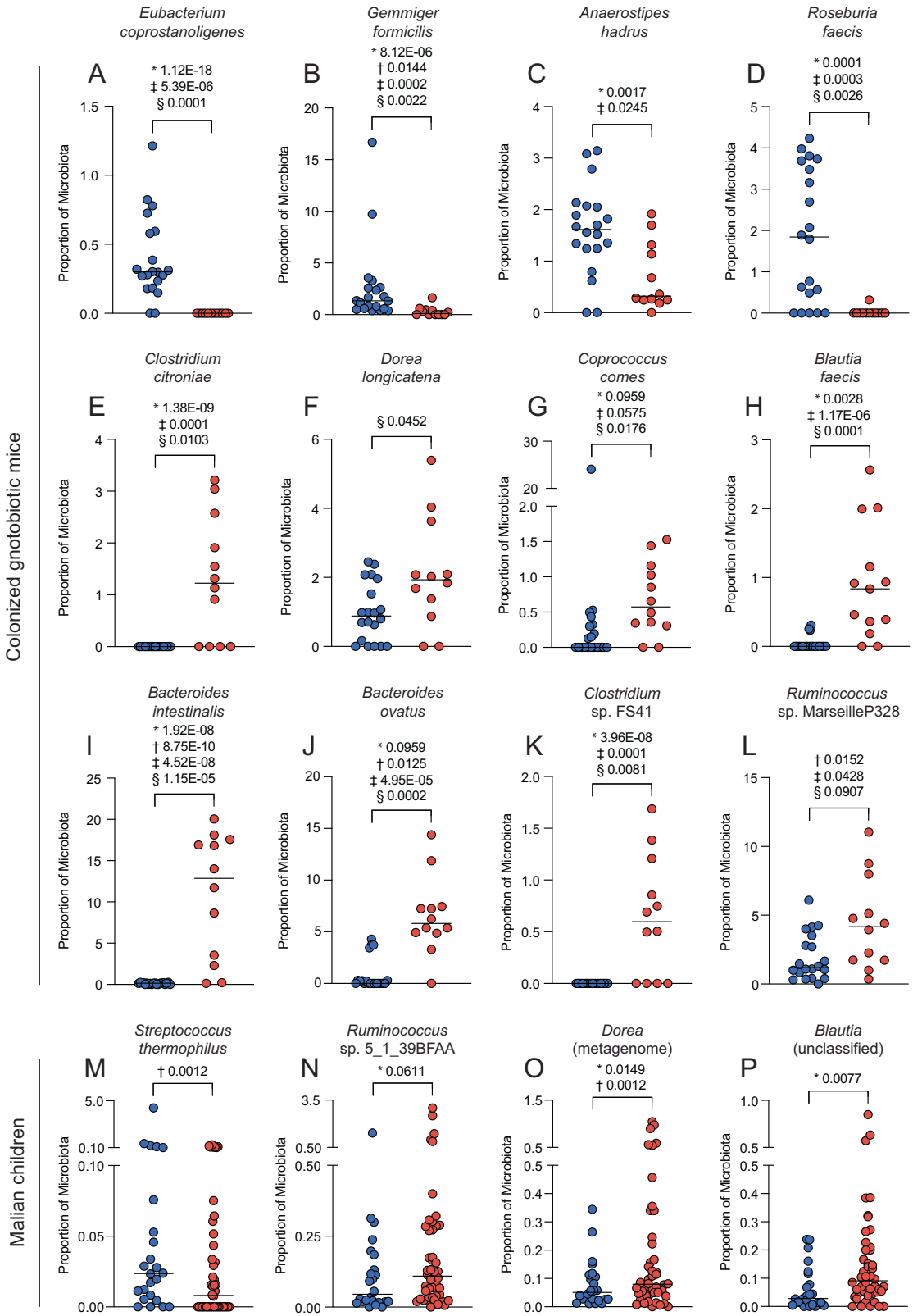

by this method. Bray–Curtis dissimilarity was significantly different ($P < 0.001$) between the resistant and susceptible groups using the shotgun metagenomic sequencing data (Supp. Fig. 2A). Furthermore, blood immune cell numbers were compared to determine if any gross differences in overall immune status were present, and no significant differences were found between the resistant and susceptible children (Supp. Fig. 2B–G).

The malaria-susceptible network is more interconnected than the resistant network

Network analysis was performed on the samples to determine if there were differential interactions between the bacteria in the resistant and susceptible children. Overall, there were three principal clusters shared by both networks; the first predominated by *Streptococcus* and *Veillonella* species, the second by *Prevotella* and *Bacteroides* species,

Fig. 2 | Taxa associated with susceptibility and resistance using 16S rRNA sequencing. Percentage of the mouse microbiome that is **A** *Eubacterium coprostanoligenes*, **B** *Gemmiger formicilis*, **C** *Anaerostipes hadrus*, **D** *Roseburia faecis*, **E** *Clostridum citroniae*, **F** *Dorea longicatena*, **G** *Coprococcus comes*, **H** *Blautia faecis*, **I** *Bacteroides intestinalis*, **J** *Bacteroides ovatus*, **K** *Clostridium* sp. FS41, and **L** *Ruminococcus* sp. Marseille-P328. Percentage of the human microbiome that is **M** *Streptococcus thermophilus*, **N** *Ruminococcus* sp. 5_1_39BFAA, **O** *Dorea* (metagenome), and **P** *Blautia* (unclassified). *P* values were determined using DESeq2 (∗), corncob (†), MaAsLin2 (‡), and ALDEx2 (§). Data were normalized using the default method for each tool: relative log expression (RLE), no normalization, total sum scaling (TSS), and no normalization, respectively, and the Benjamini–Hochberg method was used to control for multiple comparisons. Blue circles indicate resistant children or low parasitemia mice, and red circles indicate susceptible children or high parasitemia mice. Median indicated on graphs. $n = 20$ for the resistant mice and $n = 12$ for the susceptible mice. $n = 24$ for the resistant children and $n = 46$ for the susceptible children.

and the third by species in the order Eubacteriales (Fig. 3; Supp. Fig. 3). Additionally, while the edges (connections between two taxa) in the overall network were mainly positive (indicative of positive correlation between the species; 71.97% positive in the resistant network versus 66.11% positive in the susceptible network), the majority of the inter-cluster interactions were negative (indicative of negative correlation between the species; Fig. 3). The edge density (proportion of total possible edges–a measure of network connectivity) of the resistant network was only half of that of the susceptible network (0.059 versus 0.112) (Supp. Fig. 4A). A similar trend was also observed for the *Streptococcus*/*Veillonella* (0.071 versus 0.111), the *Prevotella*/*Bacteroides* (0.042 versus 0.149), and the Eubacteriales (0.096 versus 0.133) clusters individually (Supp. Fig. 4B–D).

The Jaccard index was significantly different (Jacc = 0.029; $P(J \leq j) = 0.000019$) for the two sets of hubs (the most connected taxa in each of the networks), indicating that the two sets of hubs were significantly more different than expected at random; the only shared hub was *Sellimonas intestinalis* (Supplementary Data 5). Both the resistant and susceptible networks had hubs in the Eubacteriales cluster. The susceptible network also had hubs in the *Prevotella*/*Bacteroides* cluster, and neither network had hubs in the *Streptococcus*/*Veillonella* cluster (Supplementary Data 5). Similar to what was observed for the full network, the edge density for the hubs was lower in the resistant network compared to the susceptible network (0.209 versus 0.277; Supplementary Data 5).

Interestingly, the edges connected to the hubs in the resistant network had higher absolute median edge weights (a measure of the strength of the correlation between the taxa[20]) compared to the edges connected to the hubs in the susceptible network, for both positive (0.659 versus 0.553) and negative edges (−0.616 versus −0.464) (Supp. Fig. 4E, F). Higher absolute median edge weights were also observed for the total resistant network compared to the total susceptible network (Supp. Fig. 4G, H), for both the positive (0.656 versus 0.512) and negative edges (−0.611 versus −0.443).

Bacteria in the Eubacteriales cluster are associated with malaria-susceptible children, and bacteria in the *Prevotella*/*Bacteroides* and *Streptococcus*/*Veillonella* clusters are associated with resistant children

Sparse partial least squares discriminant analysis (sPLS-DA) was performed on the metagenomics sequencing samples in order to better understand the correlation of the bacteria with each other and with susceptibility to febrile malaria. The samples were projected onto the space spanned by the first two components (Fig. 4A), which demonstrated moderate separation of the children by malaria outcome along the first component. One group of bacteria was positively correlated with component one, and one group of bacteria was negatively correlated with component one (Fig. 4B), approximately corresponding to the resistant and susceptible groups.

A closer examination of the correlation circle plot permitted a more granular characterization of the relationships between the different bacteria. The bacteria that correlated with the resistant group of children were those that were largely found within the *Prevotella*/*Bacteroides* and the *Streptococcus*/*Veillonella* clusters during network analysis (Supp. Fig. 5A). Conversely, the majority of the bacteria that correlated with the susceptible group were those that were detected in the Eubacteriales cluster (Supp. Fig. 5B). In agreement with the correlation circle plot, the bacteria with the top loading weights (a measure of how much they contribute to the component) that had a higher median abundance in the resistant group were found primarily within the *Prevotella*/*Bacteroides* and the *Streptococcus*/*Veillonella* clusters, and the bacteria that had a higher median abundance in the susceptible group were found in the Eubacteriales cluster (Fig. 4C).

Malaria susceptibility associated with Eubacteriales species using shotgun metagenomics sequencing

Differential abundance analysis was performed on the samples to determine if the disparate interaction networks within the resistant and susceptible microbiomes were associated with differential prevalence of the bacteria (Supplementary Data 6). *Prevotella copri*, *Prevotella melaninogenica*, *S. thermophilus*, *Veillonella parvula*, *Prevotella bryantii*, *Prevotella* sp. E13-17, *Petrimonas mucosa*, and *Streptococcus pneumoniae* were significantly increased in the resistant children (Fig. 5A–D; Supp. Fig. 6A–D). *Ruminococcus torques*, *Ruminococcus gauvreauii*, *Dorea formicigenerans*, *D. longicatena*, *C. comes*, *Lachnoclostridium* sp. YL32, *Lachnoclostridium phocaeense, Enterocloster clostridioformis*, *Enterocloster bolteae*, *Anaerobutyricum hallii*, *Blautia producta*, *S. intestinalis*, *Clostridium* sp. M62/1, *Clostridium scindens*, *Marvinbryantia formatexigens*, *Massilistercora timonensis*, *Blautia argi*, *Blautia liquoris*, *Blautia hansenii*, and *Butyrivibrio crossotus* were more abundant in the susceptible children (Fig. 5E–P and Supp. Fig. 6E–L).

In Ugandan children under the age of five, *Bacteroides* have been demonstrated to be significantly increased in children experiencing severe malaria anemia compared to children with an asymptomatic *P. falciparum* infection[12]. In this study, *Bacteroides caccae*, *Bacteroides cellulosilyticus*, *Bacteroides fragilis,* and *Bacteroides uniformis* were increased in the 10-year-old Malian children who were susceptible to the development of febrile symptoms (Supplementary Data 6), although this appears to be largely the result of outliers (Supp. Fig. 7A–D).

Similar to the high parasite burden mice, the susceptible children had increased abundances of bacteria that have previously been associated with mucin degradation, impaired gut barrier function, and IBD (e.g., *R. gauvreauii*, *R. torques*, *D. formicigenerans*, *D. longicatena*, *L. phocaeense* and *L.* sp. YL32)[17–19,21–23]. However, several bacteria that are known short-chain fatty acid (SCFA)-producers and that have been associated with intestinal homeostasis recovery following dysbiotic events were also significantly more abundant in the susceptible children (e.g., *A. hallii*, *B. products,* and *S. intestinalis*)[24–31].

Metabolites associated with gut barrier damage are increased in susceptible children

Since the resistant and susceptible children were shown to have differential bacterial abundance and interaction networks, untargeted metabolomics was performed to determine if these differences extended to the metabolite composition. Moderate separation of the resistant and susceptible children was observed along the first component when the samples were projected onto the space spanned by the first two components (Fig. 6A), and two groups of metabolites were observed to approximately correspond with the resistant and susceptible groups of children (Fig. 6B). The loading weights of the top

https://doi.org/10.1038/s41467-024-52953-8

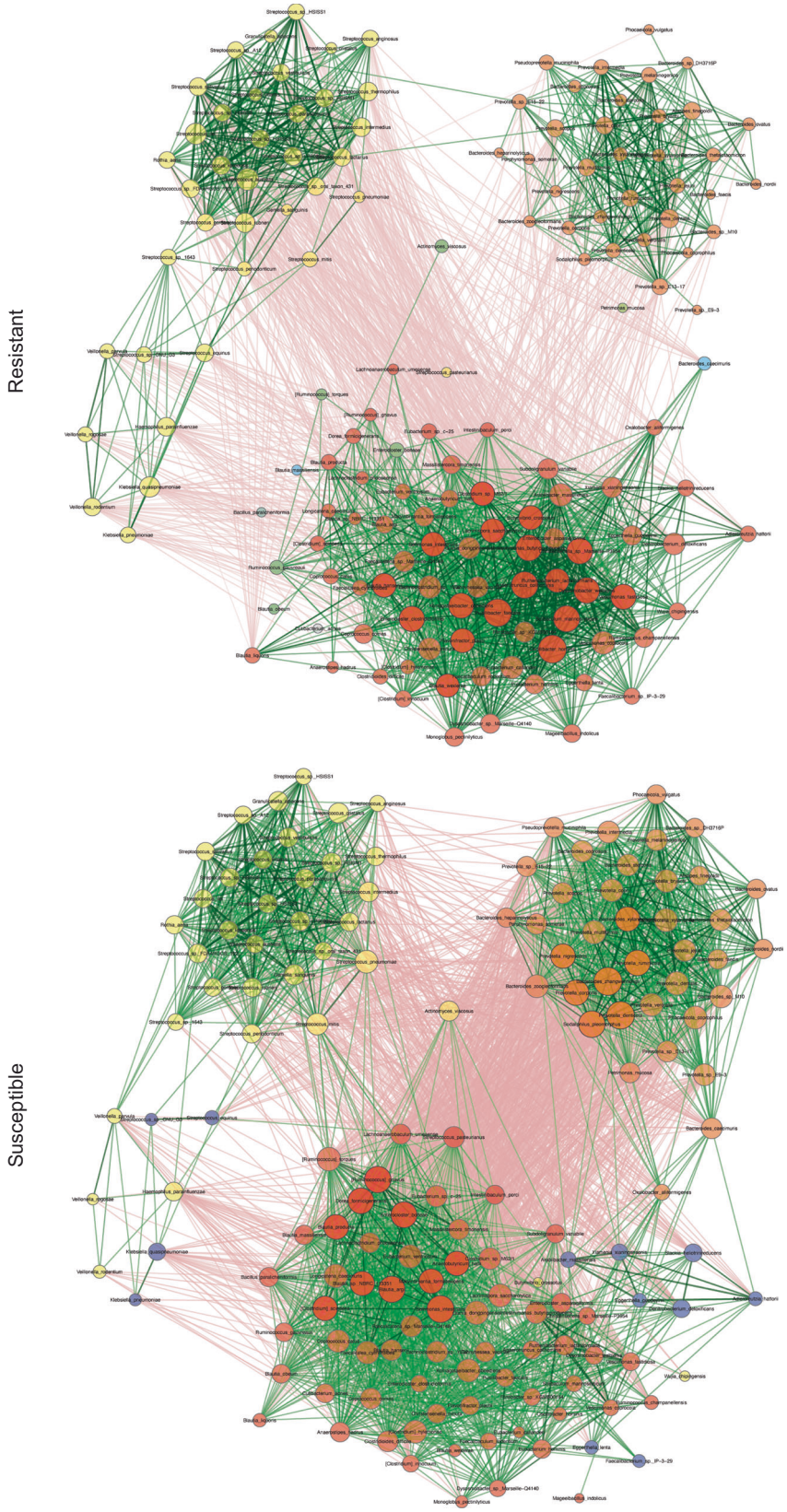

Fig. 3 | Network of the top 100 nodes by degree centrality for resistant and susceptible children. Size of nodes is indicative of degree centrality (number of connected nodes). Hubs (nodes with a degree centrality value above the empirical 95% quantile of all degree centralities in the network) are further highlighted with bold borders and decreased transparency. Nodes are colored by cluster (identified using greedy modularity optimization). Green edges indicate positive interactions, red edges indicate negative interactions, and absolute edge weight is indicated by transparency of the edge.

https://doi.org/10.1038/s41467-024-52953-8

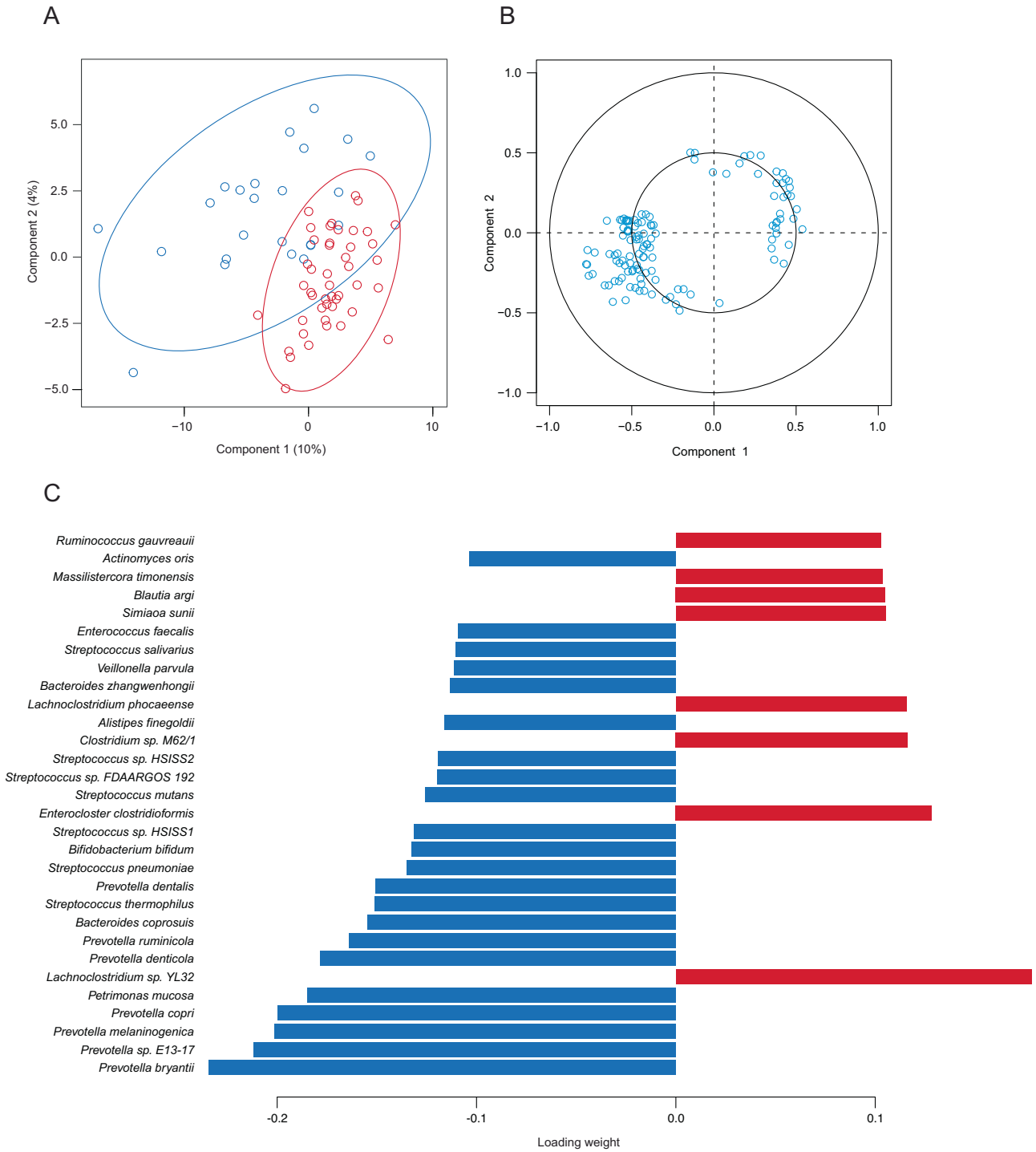

Fig. 4 | Species from the *Prevotella*/*Bacteroides* and *Streptococcus*/*Veillonella* clusters correlate with the resistant children, and species from the Eubacteriales cluster correlate with the susceptible children. A Sample plot, **B** correlation circle plot, and **C** loadings plot for the sPLS-DA of the metagenomics samples. The top 30 taxa by loading weight are listed, and the colors indicate in which group the taxa have the maximum median count—blue for the resistant group and red for the susceptible group. The ellipses represent 95% confidence intervals in the sample plot, and a correlation coefficient cutoff of 0.35 was used for the correlation circle plot.

thirty metabolites for component one were relatively evenly distributed (Fig. 6C), suggesting that the differences in metabolic activity may have been the result of comprehensive changes in pathways, rather than inordinate changes in a few select metabolites. Thus, the range of the metabolites of interest was extended to include all metabolites with an absolute loading weight of at least 0.05 (Supplementary Data 7), which brought several metabolite categories into relief.

Fifteen metabolites associated with glycerophospholipid metabolism had a higher median count in the resistant children, including sarcosine, betaine, trimethylamine-N-oxide (TMAO), trimethyllysine, stearoylcarnitine, and 9-palmitic acid hydroxystearic acid (PAHSA)/12-PAHSA, and nine phospholipids: glycerophosphorylcholine (GPC), three lysophosphatidylcholines (LPC) (1-oleoyl-GPC, 1-stearoyl-GPC, and 1-palmitoyl-GPC), glycerophosphorylethanolamine (GPE), and four lysophosphatidylethanolamines (LPE), (1-margaroyl-GPE, 1-oleoyl-

https://doi.org/10.1038/s41467-024-52953-8

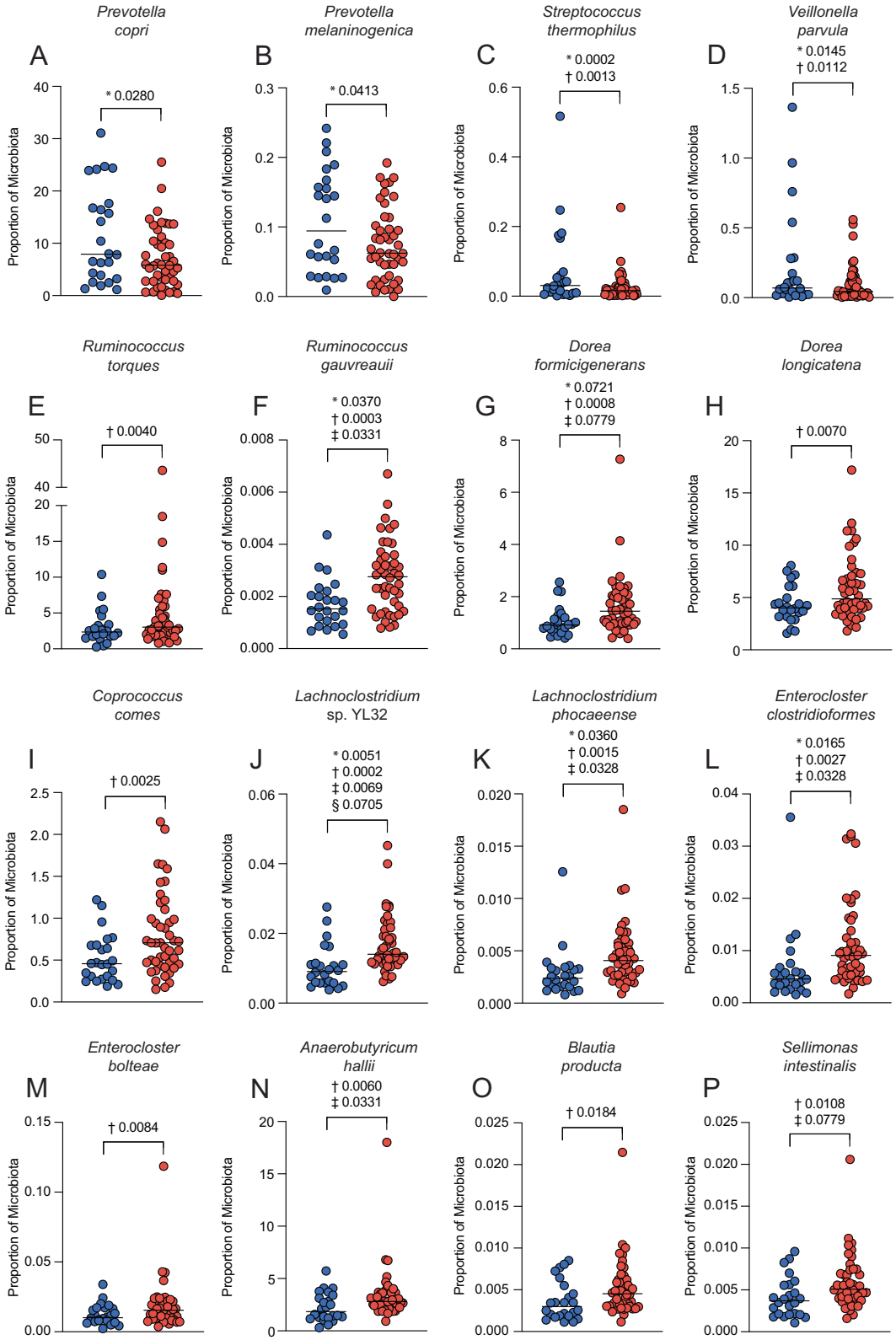

Fig. 5 | Taxa associated with susceptibility and resistance in the children using shotgun metagenomics. Percentage of the microbiome that is **A** *Prevotella copri*, **B** *Prevotella melaninogenica*, **C** *Streptococcus thermophilus*, **D** *Veillonella parvula*, **E** *Ruminococcus torques*, **F** *Ruminococcus gauvreauii*, **G** *Dorea formicigenerans*, **H** *Dorea longicatena*, **I** *Coprococcus comes*, **J** *Lachnoclostridium* sp. YL32, **K** *Lachnoclostridium phocaeense*, **L** *Enterocloster clostridioformis*, **M** *Enterocloster bolteae*, **N** *Anaerobutyricum hallii*, **O** *Blautia producta*, and **P** *Sellimonas intestinalis*. P-values determined using DESeq2 (*), corncob (†), MaAsLin2 (‡) and ALDEx2 (§). Data were normalized using the default method for each tool: relative log expression (RLE), no normalization, total sum scaling (TSS), and no normalization, respectively, and the Benjamini–Hochberg method was used to control for multiple comparisons. Blue circles indicate resistant children, and red circles indicate susceptible children. Median indicated on graphs. $n = 24$ for the resistant children and $n = 46$ for the susceptible children.

https://doi.org/10.1038/s41467-024-52953-8

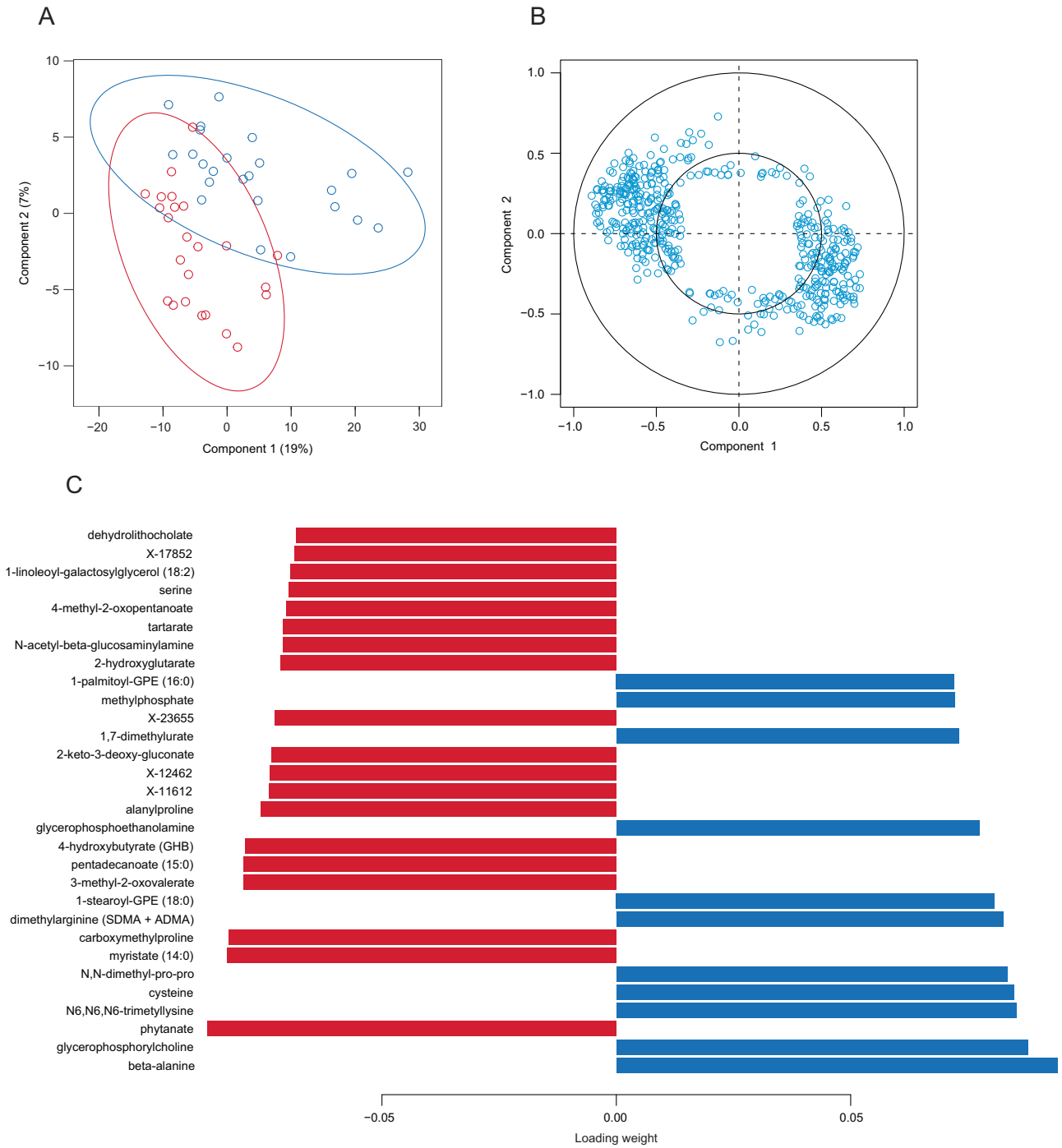

Fig. 6 | Metabolite loading weights are evenly distributed. A Sample plot, **B** correlation circle plot, and **C** loadings plot for the sPLS-DA of the metabolomics samples. The top 30 metabolites by loading weight are listed, and the colors indicate in which group the metabolite has the maximum median count—blue for the resistant group and red for the susceptible group. The ellipses represent 95% confidence intervals in the sample plot, and a correlation coefficient cut-off of 0.35 was used for the correlation circle plot.

GPE, 1-stearoyl-GPE, and 1-palmitoyl-GPE) (Supp. Fig 8A; Supp. Fig 9A–D). Interestingly, putrescine was also shown to have a higher median level in the resistant children (Supplementary Data 7), and *V. parvula*, which is more abundant in the resistant children (Fig. 5D), is known to require putrescine for growth, as it is incorporated into its peptidoglycan[32].

Eleven metabolites associated with purine and pyrimidine metabolism had higher median counts in the susceptible children: deoxyinosine, deoxyuridine, deoxycytidine, N6-methyladenosine (m6A), 5′-methyluridine (m5U), pseudouridine, xanthine, hypoxanthine, thymidine, thymine and orotate (Supp. Fig 8B; Supp. Fig 9 E-H). In addition to the metabolites associated with nucleotide metabolism, five long chain fatty acids (LCFA) (myristoleate, 10-nonadecenoate, myristate, margarate and pentadecanoate), three sterols (lanosterol, 4-cholesten-3-one and coprostanol), and eighteen unknown metabolites (Supplementary Data 7; Supp. Fig 9I–P) were additionally correlated with the susceptible children. Many of the unknown metabolites grouped together on the correlation circle plot, indicating a high level of positive correlation and potentially a shared metabolic pathway (Supp. Fig 10).

https://doi.org/10.1038/s41467-024-52953-8

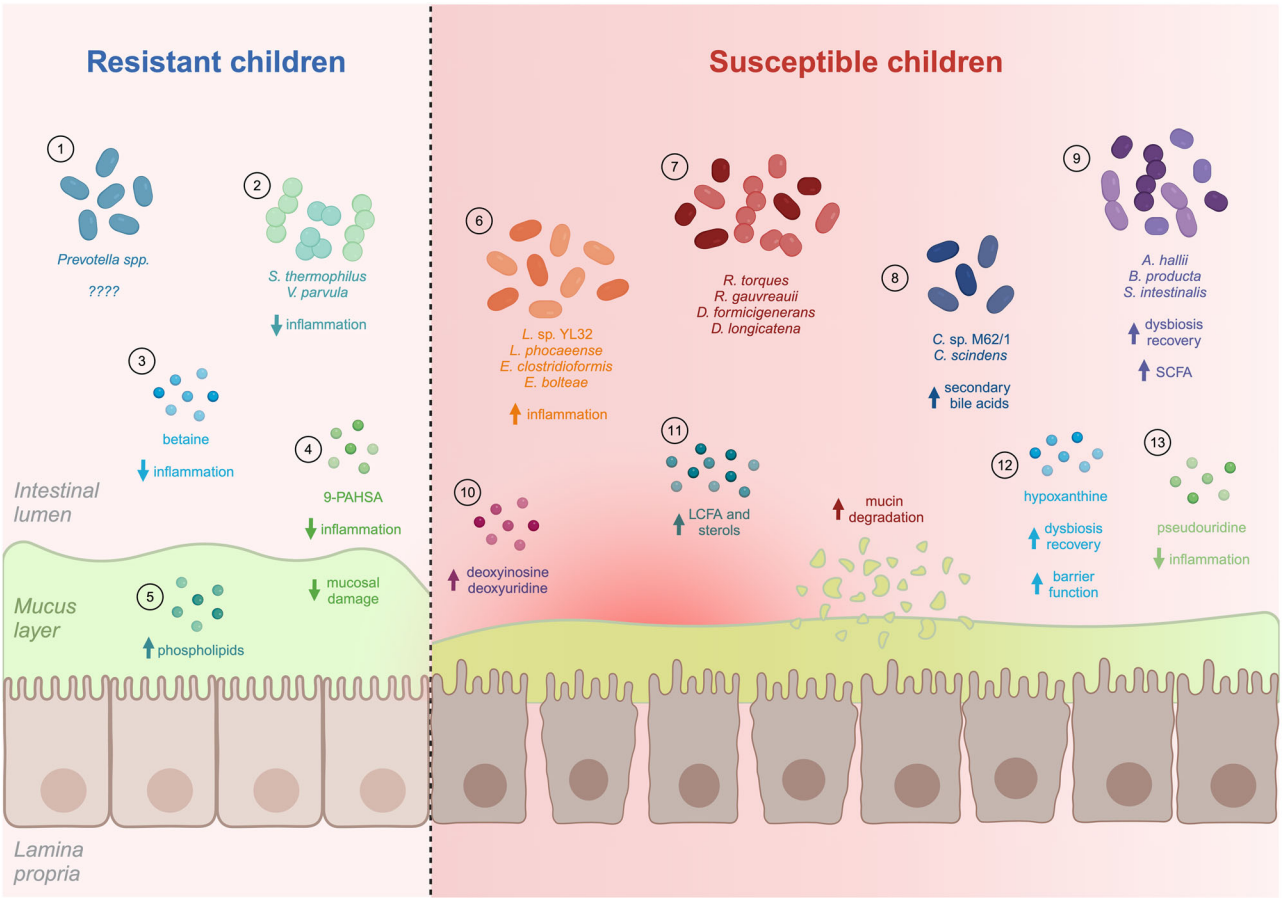

Fig. 7 | Features associated with inflammation and impaired gut barrier function are enriched in children susceptible to febrile malaria symptoms. Created with BioRender.com.

Consistent with the potential metabolic activity suggested by the shotgun metagenomics data, the metabolomics data also supported the potential presence of nitrosative stress and impaired gut barrier function (e.g., deoxyinosine and deoxyuridine) within the susceptible children[33–36], as well as the potential existence of an anti-inflammatory recovery component (e.g., hypoxanthine and pseudouridine)[37–39].

Discussion

Malaria remains a major cause of morbidity and mortality in low- and middle-income countries. Individuals living in areas with moderate-to-high *P. falciparum* transmission typically develop protection from febrile symptoms by early adolescence, but the factors underlying this transition are not well understood. We observed that the microbiome composition of 10-year-old Malian children before that start of the *Plasmodium* transmission season was significantly different between children that were resistant or susceptible to the development of febrile symptoms during the subsequent transmission season. Furthermore, gnotobiotic mice colonized with the pre-transmission season fecal sample of the susceptible children had a significantly higher parasite burden following infection with *P. yoelii* compared to gnotobiotic mice colonized with the pre-transmission season fecal sample of the resistant children. Since the microbiome composition was also shown to be different between the 10-year-old children and the younger children, these results suggest that the microbiome may be playing a role in the age-dependent protection against febrile symptoms that is observed in areas with moderate-to-high levels of *Plasmodium* transmission.

Network analysis of the shotgun metagenomics data from the human fecal samples revealed three principal clusters shared by both the resistant and the susceptible microbiomes: the first predominated by *Streptococcus* and *Veillonella* species, the second by *Prevotella* and *Bacteroides* species, and the third by species in the order Eubacteriales. The susceptible network was more interconnected than the resistant microbiome (higher edge density); however, the average strength of the individual interactions was greater in the resistant network (higher edge weights). The lower number of relatively stronger correlations between the bacteria in the resistant network is potentially indicative of metabolic interactions that are more specific and tightly controlled, while the high number of low strength correlations in the susceptible network may be suggestive of the bacteria responding more generally to an environmental change within the colon. The sPLS-DA and the differential abundance analysis of the shotgun metagenomics data found that the majority of the bacteria that were associated with/significantly more abundant in the resistant children were from the genera *Prevotella*, *Streptococcus* and *Veillonella*, while the majority of the bacteria that were associated with/significantly more abundant in the susceptible children were from the order Eubacteriales.

P. copri, which was more abundant in the resistant children using shotgun metagenomics, has been associated with contradictory impacts on human health, likely due to the high genetic diversity present within this species[40–42]. The different strains within the *P. copri* complex have been linked to country of origin and fiber intake and are associated with substantial functional diversity[41,42]. Higher fiber levels have been shown to correlate with increased potential for the degradation of complex carbohydrates by this species, whereas omnivore diets have been linked to an increased incidence of metabolic syndrome in individuals with higher levels of *P. copri*[43,44]. Several *Prevotella*-associated operational taxonomic units (OTUs) were also

found to be differentially abundant in the human 16S rRNA sequencing data, but it is difficult to make direct comparisons with the shotgun metagenomics sequencing, as the human 16S rRNA data was classified using the SILVA database, which divides *Prevotellaceae* into multiple non-monophyletic groups, each of which are associated with several individual OTUs.

S. thermophilus, which was found to be significantly increased in the resistant children by both shotgun metagenomics and 16S rRNA sequencing, has been shown to be capable of reducing inflammation in a murine model of sepsis[45]. Moreover, *V. parvula*, which was also increased in the resistant children, has been shown to modulate the immune response in in vitro co-stimulation experiments with different strains of *Streptococcus*[46]. Thus, the increased abundance of *S. thermophilus* and *V. parvula* suggests that the intestinal environment of the resistant children may have been less inflammatory than that of the susceptible children (Fig. 7).

The species associated with low parasite burden in the mice were different than those associated with resistance to febrile malaria in the children. *G. formicilis*, *A. hadrus* and *R. faecis*, which were increased in the low parasite burden mice, are known producers of SCFA, which promote gut barrier integrity and reduce inflammation[47–49]. Furthermore, *G. formicilis*, *A. hadrus*, and *R. faecis* have additionally been shown to be increased in healthy controls compared to ulcerative colitis (UC) and Crohn's disease (CD), irritable bowel syndrome (IBS), and CD, respectively[48–50]. Moreover, *E. coprostanoligenes*, which was also significantly more abundant in the low parasite burden mice, has been shown to be enriched by oroxylin A treatment in conjunction with improved protection of the colonic mucus barrier and alleviation of colitis in mice[51].

Many of the bacteria that were more abundant in the susceptible children have been associated with inflammation, impaired gut barrier function, and IBD (Fig. 7). *R. torques*, *R. gauvreauii*, *D. formicigenerans* and *D. longicatena* are mucolytic bacteria; they possess glycoside hydrolases that allow them to initiate mucin degradation by releasing the sialic acids from the non-reducing ends of glycans, impairing gut barrier function[17,18]. Accordingly, increased abundance of these bacteria has been associated with IBD[19,21–23]. *C. comes*, while not in possession of glycoside hydrolases, has also been shown to grow with mucin as the main carbon source[52] and to be enriched during IBD[19]. Additionally, *L.* sp. YL32 has been positively correlated with gut permeability and inflammation[53] and *L. phocaeense* has been shown to be enriched in patients with active IBD[54]. Finally, *E. clostridioformis* and *E. bolteae* have both been shown to be significantly enriched in CD patients[50,55].

Interestingly, the susceptible children additionally had increased abundance of several bacteria that have been shown to correspond with favorable prognosis and remission following intestinal dysbiosis (Fig. 7). *A. hallii* cannot degrade complex oligo- and polysaccharides, but participates downstream in mucin cross-feeding, and produces SCFA from mucin-derived monosaccharides[24,25]. While *A. hallii* has been shown to be enriched in IBD groups compared to control groups[19], an increased abundance of *A. hallii* and SCFA have also been associated with patients who achieved remission after fecal microbiota transplantation (FMT) treatment of UC[26], potentially suggesting that the presence of *A. hallii* during IBD is indicative of a favorable prognosis. Furthermore, an increase in SCFA has been associated with the amelioration of dextran sulfate sodium (DSS)-induced colitis in mice following oral administration of *B. producta*[27], and *S. intestinalis* has been shown to be increased in patients during homeostasis recovery following dysbiosis events[28–31].

Achievement of remission after FMT treatment of UC has additionally been associated with increased levels of secondary bile acids[26], and treatment with secondary bile acids has been shown to decrease intestinal inflammation in three models of murine colitis[56]. *C.* sp. M62/1 has been shown to play a significant role in bile acid metabolism using in silico metabolic modeling[57], and *C. scindens*, which possesses 7α-dehydroxylases that transform primary bile acids into secondary bile acids[58], has been shown to enhance resistance to *Clostridum difficile* infection in a secondary bile acid-dependent manner[59].

D. longicatena and *C. comes* were the only species associated with susceptibility in the Malian children that were also associated with high parasite burden in the colonized mice. However, despite the taxonomical differences, the bacteria that were more abundant in the high parasite burden mice have also been associated with impaired barrier function, suggesting that the high parasite burden phenotype engendered in the colonized mice may have been the product of similar metabolic activities to that which was associated with susceptibility in the children, but with a mouse specific microbiome composition. Gavage with *B. intestinalis* following antibiotic depletion of the gut microbiota has been shown to increase ileal damage compared to mice allowed to naturally repopulate their gut microbiota[60], and *C. citroniae* possesses D-cysteine desulfhydrases, which increase the concentration of colonic sulfides, potentially inhibiting the utilization of butyrate by intestinal epithelial cells[61]. Additionally, similar to the susceptible children, the high parasite burden mice also had an increased abundance of bacteria previously associated with decreased inflammatory responses: *B. ovatus* has been shown to reduce mucosal inflammation during DSS-induced colitis[62,63] and *B. faecis* has been shown to be reduced in patients with CD and to produce SCFA[49].

Congruent with the potential metabolic activity suggested by the shotgun metagenomics data, many of the metabolites associated with the susceptible children are related to inflammatory responses and gut barrier damage (Fig. 7). Deoxyinosine and deoxyuridine are DNA adducts formed through nitrosative deamination, which occurs due to the generation of nitric oxide during chronic inflammation[33], and are thus potential biomarkers of inflammatory processes. m6A is a post-transcriptional RNA modification that is influenced by the microbiota[64] and has been shown to be involved in the initiation and pathogenesis of IBD[65]. Moreover, the increased levels of LCFAs and sterols in the susceptible children further support an inflammatory intestinal environment and impaired gut barrier function, as cats with chronic inflammatory digestive disorders have been shown to have higher levels of LCFAs and animal-derived sterols in their feces compared to healthy cats[34], and LPS-induced inflammation has been shown to inhibit the absorption of LCFA by intestinal epithelial cells, concomitant with an increase in m6A modification levels[35].

Nevertheless, similar to what was suggested by the shotgun metagenomics data, the metabolomics data also supported the potential presence of a dysbiosis recovery component in the susceptible children (Fig. 7). Pseudouridine modification has been shown to be dynamically regulated in response to cellular stress and artificial pseudouridylation has been shown to reduce immune stimulation in vitro[37]. Additionally, hypoxanthine has been shown to be lower in the fecal samples of IBD patients compared to healthy controls[38] and to promote intestinal barrier function and recovery following injury or hypoxia[39]. These results suggest that while the susceptible children may have increased abundance of bacteria and metabolites associated with inflammation and gut barrier damage, there may also be additional supplementary mechanisms in place to prevent excessive damage and/or allow recovery.

Accordingly, the metabolites that were increased in the resistant children have previously been associated with decreased inflammation and improved gut barrier function (Fig. 7). Mucus phospholipids contribute to the maintenance of the intestinal mucus barrier[36], thus the increased amounts of phospholipids in the resistant children may be indicative of a more impregnable mucosal barrier. Moreover, GPC and LPE have been shown to be decreased in UC and CD patients[21,66] and LPC has been shown to be decreased in UC patients[36,67]. Finally, betaine treatment has been shown to attenuate inflammation and upregulate tight junction proteins during DSS-induced colitis[68], and

9-PAHSA has been shown to attenuate the immune response and prevent mucosal damage during DSS-induced colitis[69].

There are important limitations of the current study that warrant consideration. The current study identified associations between numerous bacteria and fecal metabolites with *P. falciparum* infection outcomes. Plausible connections between these bacteria and metabolites with intestinal inflammation status are supported by prior research. However, it is not known within this cohort if there were differences in intestinal inflammation and susceptibility to febrile malaria. Future observational and longitudinal studies in humans combined with mechanistic studies in mice will be required to demonstrate causal roles for these bacteria and metabolites with *P. falciparum* infection outcomes. Additionally, other microbiome-dependent factors (e.g., nutrient levels such purine nucleotides) could have contributed to susceptibility to febrile malaria in these 10-year-old children. Collectively, these results and associated limitations, highlight the need for ongoing investigation into the effect of gut microbiota on malaria in children.

Overall, this study demonstrated that the microbiome of 10-year-old Malian children prospectively correlates with susceptibility to the development of febrile malaria. Since the gut microbiome of the 10-year-old children was shown to be different than that of the younger children, these results suggest that the microbiome may play a role in the age-dependent protection against febrile symptoms that is observed in areas with moderate-to-high levels of *Plasmodium* transmission. Bacteria and metabolites associated with increased inflammation and gut barrier impairment were enriched within the gut microbiome of the susceptible children; however, the metagenomics and metabolomic data also indicated that the microbiome of the susceptible children also possessed features associated with recovery from dysbiosis. Further investigation into the differences in microbiome composition has the potential to lead to interventions that limit malaria morbidity.

Methods

Study design, participants, and detection of *P. falciparum* infection

181 children aged 6 to 10 years old were enrolled in a prospective cohort study from May 2014 to March 2015 conducted in Kalifabougou, Mali. A detailed description of this cohort[70] and of the composition of the typical diet consumed at the study site[71] have been previously published. The Ethics Committee of the Faculty of Medicine, Pharmacy and Dentistry at the University of Sciences, Techniques and Technology of Bamako and the Institutional Review Board of the National Institute of Allergy and Infectious Disease, National Institutes of Health approved this study (ClinicalTrials.gov identifier: NCT01322581). Written, informed consent was obtained from the parents and/or guardians of participating children. To detect asymptomatic *P. falciparum* infections, fingerprick blood samples were collected at monthly scheduled visits and PCR was performed on the dried blood spots as described previously[72]. Positive *P. falciparum* PCRs were considered to represent an asymptomatic infection if there were no reported febrile symptoms for at least 3 weeks following the PCR. Children were considered to have had a febrile malaria infection if they presented to the clinic with fever and *P. falciparum* parasites were detected by microscopic examination of blood smears. White blood cells were measured using the ABX Micros 60 (HORIBA ABX SAS). Aliquots of stool collected during the prospective cohort study were cryopreserved at −80 °C in Mali and shipped to the U.S. on dry ice for analysis.

Mouse husbandry and gnotobiotic experiment

GF, female and male C57BL/6 N mice (5-8 weeks old) were purchased from Charles River Laboratories. Mice were housed in autoclaved Tecniplast IsoCage P cages (Tecniplast Group) with ALPHA-dri bedding (Shepherd Specialty Papers, Inc) and Bed-r'Nest nesting material (The Andersons Plant Nutrient Group) under a strict 12 hr light cycle. Cages were changed once every two weeks. The mice were provided *ad libitum* with autoclaved reverse osmosis water and autoclaved 7013 (NIH-31 Modified Open Formula Mouse/Rat Sterilizable Diet) purchased from Inotiv/Envigo. Cages were submerged in a tank of Exspor for 5 min before being opened within an Exspor-sterilized biosafety cabinet (40 min contact time). Additionally, all items used with the mice (*e.g.*, gavage needles) were autoclaved and their packaging wiped down with Exspor before being transferred into the biosafety cabinet. Fecal samples were collected upon arrival and from the sentinels at the end of the experiment and sterility verified by IDEXX BioAnalytics through generic bacteria 16S rRNA gene PCR, and fungal, and aerobic and anaerobic bacteria culture (case numbers 120118-2022 and 125378-2022). All animal experiments were carried out at Indiana University adhering to the local and national regulation of laboratory animal welfare, and all procedures were reviewed and approved by the Indiana University Institutional Animal Care and Use Committees (protocol numbers 19024 and 22010).

May stool samples for the participants with the subject identification numbers 375, 400, 404, 415, 417, 446, 450 and 452 were selected to colonize the gnotobiotic mice. A portion of each fecal sample was scraped off while on dry ice and diluted in sterile saline at 1:10 (w/v). The fecal suspension was vortexed, and the larger particles allowed to settle on ice before the supernatant was collected. 200 µL of each fecal suspension was gavaged into four mice each at weekly intervals for four weeks, as was previously described[71]. A four-week regime was used to colonize the mice as previous studies have shown that during conventionalization of mice microbial communities undergo ecological succession (they transition through various pioneering communities) before achieving compositional stability after approximately four weeks[73,74], and a four-week regime has also been shown to produce the most stable colonization of human fecal microbiota within mice[71,75,76]. Fecal samples were collected from the colonized mice on the day of infection and were flash frozen in liquid nitrogen and stored at −80 °C. This approach resulted in 85% of genus-level taxa in Malian stool samples detected in mouse fecal pellets (data not shown).

Mice were infected with *P. yoelii* 17XNL by intraperitoneal injection of 1.5×10^5 parasitized red blood cells prepared from fresh donor mouse blood. Tail vein blood was collected on days 5, 7, 9, 12, 14, 16, 19, 21 and 23 post-infection to monitor parasitemia (Fig. 1E). The blood was stained with CD45.2-APC (1:200; clone 104; BioLegend), TER-119-APC/Cy7 (1:400; clone TER-119; BioLegend), dihydroethidium (5 mg/mL stock at 1:500; MilliporeSigma), and Hoechst 34580 (1 mg/mL stock at 1:1000; MilliporeSigma) and parasitemia evaluated using flow cytometry on the Attune NxT (Thermo Fisher Scientific). Samples were analyzed with FlowJo v10.8.1 (Tree Star), and parasitized red blood cells were defined as CD45.2− TER-119$^+$ dihydroethidium$^+$ Hoechst$^+$ cells (Supp. Fig 11).

DNA sequencing and feature table construction

DNA isolation and sequencing for the human 16S rRNA sequence data was performed by the J. Craig Venter Institute (JCVI). The V4 region of the 16S rRNA gene was amplified using the 515 F (GTGCCAGCMGCCGCGGTAA) and 806 R (GGACTACHVGGGTWTCTAAT) primer pair and sequenced using an Illumina MiSeq. An in-house pipeline was used by JCVI to construct the feature table, using the SILVA SSU Ref NR99 database (v123) for taxonomic classification. For the mouse 16S rRNA sequencing and the human shotgun metagenomics sequencing, DNA was extracted from the feces using the QIAamp PowerFecal DNA kit (QIAGEN, Germantown, MD) according to the manufacturer's instructions. For the mouse 16S rRNA sequencing, the DNA samples were shipped overnight on ice packs to the Genome Technology Access Center (GTAC; Washington University, St. Louis, MO) for 16S rRNA gene sequencing using Multiple

16S Variable Region Species-level Identification (MVRSION), an approach that sequences all 9 hypervariable regions of the 16S rRNA gene with 14 primer pairs[77]. The OTU table was constructed by GTAC and imported into QIIME2[78]. For the human shotgun metagenomics sequencing, the DNA library preparation and sequencing was performed by the Center for Medical Genomics (CMG) at the Indiana University School of Medicine using the Nextera XT DNA Library Preparation Kit (Illumina) and the NovaSeq 6000 with 150 bp paired-end sequencing. Quality control and host sequence removal was performed using KneadData (v0.12.0)[79]. Briefly, FastQC (v0.11.9)[80] removed overrepresented sequences (>0.1% frequency), Trimmomatic (v0.33)[81] removed low quality reads and adapters (SLIDINGWINDOW:4:20 MINLEN: 50), TRF (v4.09.1)[82] removed tandem repeats, and bowtie2 (v2.5.1)[83] mapped the samples to the human genome assembly GRCh37 (hg37) to remove possible human read contamination. The feature table was created using Kraken2 (v2.1.2)[84] and Bracken (v2.8.0)[85] with the pre-built standard Kraken2 database (version k2_standard_20230314). Minimum hit groups was increased to 4 and the confidence score was increased to 0.10.

Metabolomics

The fecal samples were shipped overnight to Metabolon on dry ice and maintained at −80 °C at Metabolon until processing. Fecal samples were lysophilized and normalized by changing the extract volume so that a constant dry mass was extracted from all samples by collecting a fixed volume. Briefly, samples were prepared using the automated MicroLab STAR® system from Hamilton Company. Proteins were precipitated with methanol and vigorous shaking for 2 min (Glen Mills GenoGrinder 2000) followed be centrifugation. The samples were then divided into multiple fractions: two fractions for analysis by two separate reverse phase/UPLC-MS/MS methods with positive ion mode electrospray ionization, one fraction for analysis by reverse phase/UPLC-MS/MS with negative ion mode electrospray ionization, and one fraction for analysis by HILIC/UPLC-MS/MS with negative ion mode ESI. Organic solvent was removed using a TurboVap® (Zymark) and the samples stored under nitrogen until analysis. The dried samples were reconstituted in different solvents according to the four methods. Each of the four methods used a Waters ACQUITY ultra-performance liquid chromatography (UPLC) and a Thermo Scientific Q-Exactive high resolution/accurate mass spectrometer interfaced with a heated electrospray ionization (HESI-II) source and Orbitrap mass analyzer operated at 35,000 mass resolution. Two aliquots were analyzed using acidic positive ion conditions, one chromatographically optimized for more hydrophilic compounds (PosEarly; gradient eluted from a C18 column (Waters UPLC BEH C18-2.1x100mm, 1.7 μm) using water and methanol, containing 0.05% perfluoropentanoic acid (PFPA) and 0.1% formic acid (FA)) and the other chromatographically optimized for more hydrophobic compounds (PosLate; gradient eluted from the same C18 column as PosEarly using methanol, acetonitrile, water, 0.05% PFPA and 0.01% FA). The third aliquot was analyzed using basic negative ion optimized conditions (Neg; gradient eluted from a separate dedicated C18 column using methanol and water with 6.5 mM ammoninum bicarbonate at pH 8), and the fourth aliquot was analyzed via negative ionization following elution from a HILIC column (Waters UPLC BEH Amide 2.1 × 150 mm, 1.7 μm; HILIC; gradient eluted using water and acetonitrile with 10 mM ammonium formate, pH 10.8). The MS analysis alternated between MS and data-dependent MS^n scans using dynamic exclusion. The scan range varied slightly between methods but covered 70–1000 m/z. Raw data was extracted, peak-identified and quality control processed using a combination of Metabolon developed software services.

Statistics and reproducibility

Exclusion criteria for the prospective cohort study included a hemoglobin level <7 g/dL, axillary temperature ≥37.5 °C accompanied by *Plasmodium* parasites detected by either microscope or PCR, underlying chronic disease, or the use of antibiotics or immunosuppressants in the preceding 6 months. Two children were additionally removed from this study due to missing fecal samples. Twenty-three children were excluded from further analysis because they had no detected *P. falciparum* infections during the study period by microscopy or by PCR, leaving a total of 156 children for microbiome analysis (Supplementary Data 1).

Sex composition was not significantly different between the resistant and susceptible children (Fisher's exact test; $P = 0.8009$), therefore sex was not controlled for in the following analyses.

Cumulative sum scaling[86] was used to normalize the mouse and human 16S rRNA sequencing feature tables, and relative log expression[87] was used to normalize the human shotgun metagenomics sequencing feature table. Bray-Curtis diversity was calculated using the default settings in QIIME2 (v2022.11.1)[78] without rarefaction.

Mouse and human 16S rRNA sequencing and human shotgun metagenomics sequencing feature tables underwent differential abundance analysis using DESeq2[87], corncob[88], MaAsLin2[89], and ALDEx2[90]. Feature tables were normalized using the default method for each tool: relative log expression (RLE), no normalization, total sum scaling (TSS), and no normalization, respectively, and the Benjamini–Hochberg method was used to control for multiple comparisons.

Network analysis was performed on the human shotgun metagenomics sequencing feature table using the NetCoMi package[20] (default settings were used). Associations between taxa were computed using SparCC[91]. SparCC estimates the correlations between the taxa from log-ratio-transformed variances via an approximation based on the assumption that the underlying network is sparse (taxa are uncorrelated on average). Zeros are handled through a Bayesian approach (observations replaced by random sampling), and nested iterations are used to reinforce the sparsity assumption and to account for the uncertainty due to the random sampling. The calculated associations were sparsified (two-sided *t* test) and transformed into similarities that were used to build the association networks. Hubs were determined by degree centrality (number of connected nodes) and clusters (densely connected nodes that are sparsely connected to other clusters) were determined using fast greedy modularity optimization[92] provided by the igraph package[93].

We applied sPLS-DA (Sparse Partial Least Square–Discriminant Analysis)[94,95] to select taxa and/or metabolites that are important for discriminating resistant and susceptible microbiomes. We note here that our intent was to discover microbial related features that aid in understanding phenotypic differences, rather than building a classification tool for phenotype prediction. Thus, we chose sPLS-DA over other more recent ML/AI tools for the simplicity and the interpretability of the provided results.

sPLS-DA assumes that the majority of features are uninformative in the characterization of the different groups, thus a tuning step is performed to select a smaller subset of features[95]. The classification error rate (balanced error rate) was estimated with respect to the number of features selected (a sequence equal to c(1:10, seq(15, 350, 5)) for the metagenomics analysis and a sequence equal to c(1:10, seq(15, 790, 15)) for the metabolomics analysis), using 12-fold (metagenomics) and 8-fold cross-validation (metabolomics) repeated 50 times for the first five components. The minimum classification error rate was achieved with one component and 160 taxa for the metagenomics analysis and with one component and 765 metabolites for the metabolomics analysis, assessed with a one-sided t-test. Two components were used for visualization purposes. The human shotgun metagenomics sequencing feature table was normalized using RLE[87] and MetaboAnalystR[96] was used to normalize and transform the metabolomics feature table (normalization by median and log10 transformation).

The statistical significance of the difference in the area under the curve for the parasitemia was determined using a two-sided Mann Whitney U test in GraphPad Prism v9.4.1.

No statistical method was used to predetermine sample size. The experiments were not randomized. The investigators were not blinded to allocation during experiments and outcome assessment.

Reporting summary

Further information on research design is available in the Nature Portfolio Reporting Summary linked to this article.

Data availability

The data generated in this study have been deposited in the NCBI Sequence Read Archive and EMBL-EBI MetaboLights databases under the accession codes: PRJNA417939, PRJNA1096289, PRJNA1096327, and MTBLS2247.

Code availability

All feature tables and analysis scripts produced as part of this study can be found in the GitHub repository: https://github.com/kmvanden/microbiome_malaria_Mali.

References

1. World Malaria Report. (World Health Organization, Geneva, 2023).
2. Lindblade, K. A., Steinhardt, L., Samuels, A., Kachur, S. P. & Slutsker, L. The silent threat: asymptomatic parasitemia and malaria transmission. *Expert Rev. Anti Infect. Ther.* **11**, 623–639 (2013).
3. Filipe, J. A., Riley, E. M., Drakeley, C. J., Sutherland, C. J. & Ghani, A. C. Determination of the processes driving the acquisition of immunity to malaria using a mathematical transmission model. *PLoS Comput. Biol.* **3**, e255 (2007).
4. Dondorp, A. M. et al. The relationship between age and the manifestations of and mortality associated with severe malaria. *Clin. Infect. Dis.* **47**, 151–157 (2008).
5. von Seidlein, L. et al. Predicting the clinical outcome of severe falciparum malaria in african children: findings from a large randomized trial. *Clin. Infect. Dis.* **54**, 1080–1090 (2012).
6. Qin, J. et al. A metagenome-wide association study of gut microbiota in type 2 diabetes. *Nature* **490**, 55–60 (2012).
7. Morgan, X. C. et al. Dysfunction of the intestinal microbiome in inflammatory bowel disease and treatment. *Genome Biol.* **13**, R79 (2012).
8. Jangi, S. et al. Alterations of the human gut microbiome in multiple sclerosis. *Nat. Commun.* **7**, 12015 (2016).
9. Britton, R. A. & Young, V. B. Role of the intestinal microbiota in resistance to colonization by Clostridium difficile. *Gastroenterology* **146**, 1547–1553 (2014).
10. Villarino, N. F. et al. Composition of the gut microbiota modulates the severity of malaria. *Proc. Natl. Acad. Sci. USA* **113**, 2235–2240 (2016).
11. Ichinohe, T. et al. Microbiota regulates immune defense against respiratory tract influenza A virus infection. *Proc. Natl. Acad. Sci. USA* **108**, 5354–5359 (2011).
12. Mandal, R. K. et al. Gut Bacteroides act in a microbial consortium to cause susceptibility to severe malaria. *Nat. Commun.* **14**, 6465 (2023).
13. Mandal, R. K. et al. Dynamic modulation of spleen germinal center reactions by gut bacteria during Plasmodium infection. *Cell Rep.* **35**, 109094 (2021).
14. Yooseph, S. et al. Stool microbiota composition is associated with the prospective risk of Plasmodium falciparum infection. *BMC Genomics* **16**, 631 (2015).
15. Yatsunenko, T. et al. Human gut microbiome viewed across age and geography. *Nature* **486**, 222–227 (2012).
16. Portugal, S. et al. Treatment of chronic asymptomatic plasmodium falciparum infection does not increase the risk of clinical malaria upon reinfection. *Clin. Infect. Dis.* **64**, 645–653 (2017).
17. Tailford, L. E., Crost, E. H., Kavanaugh, D. & Juge, N. Mucin glycan foraging in the human gut microbiome. *Front. Genet.* **6**, 81 (2015).
18. Vacca, M. et al. The controversial role of human gut lachnospiraceae. *Microorganisms* **8**, 573 (2020).
19. Bakir-Gungor, B. et al. Inflammatory bowel disease biomarkers of human gut microbiota selected via different feature selection methods. *PeerJ* **10**, e13205 (2022).
20. Peschel, S., Müller, C. L., von Mutius, E., Boulesteix, A.-L. & Depner, M. NetCoMi: network construction and comparison for microbiome data in R. *Brief. Bioinform.* **22**, bbaa290 (2020).
21. Lloyd-Price, J. et al. Multi-omics of the gut microbial ecosystem in inflammatory bowel diseases. *Nature* **569**, 655–662 (2019).
22. Png, C. W. et al. Mucolytic bacteria with increased prevalence in IBD mucosa augment in vitro utilization of mucin by other bacteria. *Am. J. Gastroenterol.* **105**, 2420–2428 (2010).
23. Rajilić-Stojanović, M. et al. Global and deep molecular analysis of microbiota signatures in fecal samples from patients with irritable bowel syndrome. *Gastroenterology* **141**, 1792–1801 (2011).
24. Bunesova, V., Lacroix, C. & Schwab, C. Mucin cross-feeding of infant bifidobacteria and eubacterium hallii. *Microb. Ecol.* **75**, 228–238 (2018).
25. Duncan, S. H., Louis, P. & Flint, H. J. Lactate-utilizing bacteria, isolated from human feces, that produce butyrate as a major fermentation product. *Appl. Environ. Microbiol* **70**, 5810–5817 (2004).
26. Paramsothy, S. et al. Specific bacteria and metabolites associated with response to fecal microbiota transplantation in patients with ulcerative colitis. *Gastroenterology* **156**, 1440–1454.e1442 (2019).
27. Mao, B. et al. Blautia producta displays potential probiotic properties against dextran sulfate sodium-induced colitis in mice. *Food Sci. Hum. Wellness* **13**, 709–720 (2024).
28. Muñoz, M. et al. Comprehensive genome analyses of Sellimonas intestinalis, a potential biomarker of homeostasis gut recovery. *Micro. Genom.* **6**, mgen000476 (2020).
29. Kong, C. et al. Alterations in intestinal microbiota of colorectal cancer patients receiving radical surgery combined with adjuvant CapeOx therapy. *Sci. China Life Sci.* **62**, 1178–1193 (2019).
30. Liu, Y. et al. Splenectomy leads to amelioration of altered gut microbiota and metabolome in liver cirrhosis patients. *Front Microbiol* **9**, 963 (2018).
31. Osaki, H. et al. Clinical response and changes in the fecal microbiota and metabolite levels after fecal microbiota transplantation in patients with inflammatory bowel disease and recurrent Clostridioides difficile infection. *Fujita Med J.* **7**, 87–98 (2021).
32. Kamio, Y. & Nakamura, K. Putrescine and cadaverine are constituents of peptidoglycan in Veillonella alcalescens and Veillonella parvula. *J. Bacteriol.* **169**, 2881–2884 (1987).
33. Lonkar, P. & Dedon, P. C. Reactive species and DNA damage in chronic inflammation: reconciling chemical mechanisms and biological fates. *Int. J. Cancer* **128**, 1999–2009 (2011).
34. Sung, C. H. et al. Fecal concentrations of long-chain fatty acids, sterols, and unconjugated bile acids in cats with chronic enteropathy. *Anim. (Basel)* **13**, 2753 (2023).
35. Zong, X. et al. Mettl3 deficiency sustains long-chain fatty acid absorption through suppressing Traf6-dependent inflammation response. *J. Immunol.* **202**, 567–578 (2019).
36. Braun, A. et al. Alterations of phospholipid concentration and species composition of the intestinal mucus barrier in ulcerative colitis: a clue to pathogenesis. *Inflamm. Bowel Dis.* **15**, 1705–1720 (2009).
37. Borchardt, E. K., Martinez, N. M. & Gilbert, W. V. Regulation and function of RNA pseudouridylation in human cells. *Annu. Rev. Genet.* **54**, 309–336 (2020).

38. Mars, R. A. T. et al. Longitudinal multi-omics reveals subset-specific mechanisms underlying irritable bowel syndrome. *Cell* **182**, 1460–1473.e1417 (2020).
39. Lee, J. S. et al. Hypoxanthine is a checkpoint stress metabolite in colonic epithelial energy modulation and barrier function. *J. Biol. Chem.* **293**, 6039–6051 (2018).
40. Abdelsalam, N. A., Hegazy, S. M. & Aziz, R. K. The curious case of Prevotella copri. *Gut Microbes* **15**, 2249152 (2023).
41. Tett, A. et al. The prevotella copri complex comprises four distinct clades underrepresented in westernized populations. *Cell Host Microbe* **26**, 666–679.e667 (2019).
42. De Filippis, F. et al. Distinct genetic and functional traits of human intestinal prevotella copri strains are associated with different habitual diets. *Cell Host Microbe* **25**, 444–453.e443 (2019).
43. Pedersen, H. K. et al. Human gut microbes impact host serum metabolome and insulin sensitivity. *Nature* **535**, 376–381 (2016).
44. Kovatcheva-Datchary, P. et al. Dietary fiber-induced improvement in glucose metabolism is associated with increased abundance of prevotella. *Cell Metab.* **22**, 971–982 (2015).
45. Han, F. et al. Streptococcus thermophilus attenuates inflammation in septic mice mediated by gut microbiota. *Front. Microbiol.* **11**, 598010 (2020).
46. van den Bogert, B., Meijerink, M., Zoetendal, E. G., Wells, J. M. & Kleerebezem, M. Immunomodulatory properties of Streptococcus and Veillonella isolates from the human small intestine microbiota. *PLoS One* **9**, e114277 (2014).
47. Gossling, J. & Moore, W. E. C. Gemmiger formicilis, n.gen., n.sp., an Anaerobic budding bacterium from intestines. *Int. J. Syst. Evolut. Microbiol.* **25**, 202–207 (1975).
48. Kant, R., Rasinkangas, P., Satokari, R., Pietilä, T. E. & Palva, A. Genome sequence of the butyrate-producing anaerobic bacterium anaerostipes hadrus PEL 85. *Genome Announc* **3**, e00224–15 (2015).
49. Takahashi, K. et al. Reduced abundance of butyrate-producing bacteria species in the fecal microbial community in Crohn's disease. *Digestion* **93**, 59–65 (2016).
50. Sankarasubramanian, J., Ahmad, R., Avuthu, N., Singh, A. B. & Guda, C. Gut microbiota and metabolic specificity in ulcerative colitis and Crohn's disease. *Front Med (Lausanne)* **7**, 606298 (2020).
51. Bai, D. et al. Oroxylin A maintains the colonic mucus barrier to reduce disease susceptibility by reconstituting a dietary fiber-deprived gut microbiota. *Cancer Lett.* **515**, 73–85 (2021).
52. Tramontano, M. et al. Nutritional preferences of human gut bacteria reveal their metabolic idiosyncrasies. *Nat. Microbiol.* **3**, 514–522 (2018).
53. Terefe, Y. et al. Co-occurrence of campylobacter species in children from eastern ethiopia, and their association with environmental enteric dysfunction, diarrhea, and host microbiome. *Front Public Health* **8**, 99 (2020).
54. Chandrasekaran, P. et al. Intestinal microbiome and metabolome signatures in patients with chronic granulomatous disease. *J. Allergy Clin. Immunol.* **152**, 1619–1633.e11 (2023).
55. Serrano-Gómez, G. et al. Dysbiosis and relapse-related microbiome in inflammatory bowel disease: a shotgun metagenomic approach. *Comput. Struct. Biotechnol. J.* **19**, 6481–6489 (2021).
56. Sinha, S. R. et al. Dysbiosis-induced secondary bile acid deficiency promotes intestinal inflammation. *Cell Host Microbe* **27**, 659–670.e655 (2020).
57. Heinken, A. et al. Systematic assessment of secondary bile acid metabolism in gut microbes reveals distinct metabolic capabilities in inflammatory bowel disease. *Microbiome* **7**, 75 (2019).
58. Ridlon, J. M., Kang, D. J. & Hylemon, P. B. Bile salt biotransformations by human intestinal bacteria. *J. Lipid Res.* **47**, 241–259 (2006).
59. Buffie, C. G. et al. Precision microbiome reconstitution restores bile acid mediated resistance to Clostridium difficile. *Nature* **517**, 205–208 (2015).
60. Andrews, M. C. et al. Gut microbiota signatures are associated with toxicity to combined CTLA-4 and PD-1 blockade. *Nat. Med.* **27**, 1432–1441 (2021).
61. Zhang, Y. L. et al. Gut microbiota contributes to the distinction between two traditional Chinese medicine syndromes of ulcerative colitis. *World J. Gastroenterol.* **25**, 3242–3255 (2019).
62. Ihekweazu, F. D. et al. Bacteroides ovatus ATCC 8483 monotherapy is superior to traditional fecal transplant and multi-strain bacteriotherapy in a murine colitis model. *Gut Microbes* **10**, 504–520 (2019).
63. Ihekweazu, F. D. et al. Bacteroides ovatus promotes IL-22 production and reduces trinitrobenzene sulfonic acid-driven colonic inflammation. *Am. J. Pathol.* **191**, 704–719 (2021).
64. Jabs, S. et al. Impact of the gut microbiota on the m(6)A epitranscriptome of mouse cecum and liver. *Nat. Commun.* **11**, 1344 (2020).
65. Zhang, J. et al. m6A modification in inflammatory bowel disease provides new insights into clinical applications. *Biomed. Pharmacother.* **159**, 114298 (2023).
66. Balasubramanian, K. et al. Metabolism of the colonic mucosa in patients with inflammatory bowel diseases: an in vitro proton magnetic resonance spectroscopy study. *Magn. Reson. Imaging* **27**, 79–86 (2009).
67. Tang, X. et al. Gut microbiota-mediated lysophosphatidylcholine generation promotes colitis in intestinal epithelium-specific Fut2 deficiency. *J. Biomed. Sci.* **28**, 20 (2021).
68. Zhao, N. et al. Betaine supplementation alleviates dextran sulfate sodium-induced colitis via regulating the inflammatory response, enhancing the intestinal barrier, and altering gut microbiota. *Food Funct.* **13**, 12814–12826 (2022).
69. Lee, J. et al. Branched fatty acid esters of hydroxy fatty acids (FAHFAs) protect against colitis by regulating gut innate and adaptive immune responses. *J. Biol. Chem.* **291**, 22207–22217 (2016).
70. Doumbo, S. et al. Co-infection of long-term carriers of Plasmodium falciparum with Schistosoma haematobium enhances protection from febrile malaria: a prospective cohort study in Mali. *PLoS Negl. Trop. Dis.* **8**, e3154 (2014).
71. Van Den Ham, K. M. et al. Creation of a non-Western humanized gnotobiotic mouse model through the transplantation of rural African fecal microbiota. *Microbiol. Spectr.* **11**, e0155423 (2023).
72. Tran, T. M. et al. An intensive longitudinal cohort study of Malian children and adults reveals no evidence of acquired immunity to Plasmodium falciparum infection. *Clin. Infect. Dis.* **57**, 40–47 (2013).
73. Choo, J. M. & Rogers, G. B. Establishment of murine gut microbiota in gnotobiotic mice. *iScience* **24**, 102049 (2021).
74. Gillilland, M. G. et al. Ecological succession of bacterial communities during conventionalization of germ-free mice. *Appl. Environ. Microbiol* **78**, 2359–2366 (2012).
75. Hintze, K. J. et al. Broad scope method for creating humanized animal models for animal health and disease research through antibiotic treatment and human fecal transfer. *Gut Microbes* **5**, 183–191 (2014).
76. Wrzosek, L. et al. Transplantation of human microbiota into conventional mice durably reshapes the gut microbiota. *Sci. Rep.* **8**, 6854 (2018).
77. Schriefer, A. E. et al. A multi-amplicon 16S rRNA sequencing and analysis method for improved taxonomic profiling of bacterial communities. *J. Microbiol. Methods* **154**, 6–13 (2018).
78. Bolyen, E. et al. Reproducible, interactive, scalable and extensible microbiome data science using QIIME 2. *Nat. Biotechnol.* **37**, 852–857 (2019).

79. bioBakery. KneadData User Manual, https://github.com/biobakery/kneaddata.
80. Andrews, S. O. FastQC: a quality control tool for high throughput sequence data., https://www.scienceopen.com/document?vid=de674375-ab83-4595-afa9-4c8aa9e4e736 (2010).
81. Bolger, A. M., Lohse, M. & Usadel, B. Trimmomatic: a flexible trimmer for Illumina sequence data. *Bioinformatics* **30**, 2114–2120 (2014).
82. Benson, G. Tandem repeats finder: a program to analyze DNA sequences. *Nucleic Acids Res.* **27**, 573–580 (1999).
83. Langmead, B. & Salzberg, S. L. Fast gapped-read alignment with Bowtie 2. *Nat. Methods* **9**, 357–359 (2012).
84. Wood, D. E., Lu, J. & Langmead, B. Improved metagenomic analysis with Kraken 2. *Genome Biol.* **20**, 257 (2019).
85. Lu, J. B., Thielen, F. P. & Salzberg, P. S.L. Bracken: estimating species abundance in metagenomics data. *PeerJ Comput. Sci.* **3**, e104 (2017).
86. Paulson, J. N., Stine, O. C., Bravo, H. C. & Pop, M. Differential abundance analysis for microbial marker-gene surveys. *Nat. Methods* **10**, 1200–1202 (2013).
87. Love, M. I., Huber, W. & Anders, S. Moderated estimation of fold change and dispersion for RNA-seq data with DESeq2. *Genome Biol.* **15**, 550 (2014).
88. Martin, B. D., Witten, D. & Willis, A. D. Modeling microbial abundances and dysbiosis with beta-binomial regression. *Ann. Appl. Stat.* **14**, 94–115 (2020).
89. Mallick, H. et al. Multivariable association discovery in population-scale meta-omics studies. *PLoS Comput. Biol.* **17**, e1009442 (2021).
90. Fernandes, A. D. et al. Unifying the analysis of high-throughput sequencing datasets: characterizing RNA-seq, 16S rRNA gene sequencing and selective growth experiments by compositional data analysis. *Microbiome* **2**, 15 (2014).
91. Friedman, J. & Alm, E. J. Inferring correlation networks from genomic survey data. *PLoS Comput. Biol.* **8**, e1002687 (2012).
92. Clauset, A., Newman, M. E. & Moore, C. Finding community structure in very large networks. *Phys. Rev. E Stat. Nonlin Soft Matter Phys.* **70**, 066111 (2004).
93. Csardi, G., & Nepusz, T. The igraph software package for complex network research. *InterJournal Complex Syst.* **1695**, 1–9 (2006).
94. Rohart, F., Gautier, B., Singh, A. & Lê Cao, K.-A. mixOmics: an R package for 'omics feature selection and multiple data integration. *PLoS Comput. Biol.* **13**, e1005752 (2017).
95. Lê Cao, K. A., Boitard, S. & Besse, P. Sparse PLS discriminant analysis: biologically relevant feature selection and graphical displays for multiclass problems. *BMC Bioinform.* **12**, 253 (2011).
96. Chong, J. et al. MetaboAnalyst 4.0: towards more transparent and integrative metabolomics analysis. *Nucleic Acids Res.* **46**, W486–W494 (2018).

Acknowledgements

We thank the residents of Kalifabougou, Mali for participating in this study. We thank Drs. Yuzhen Ye and Andrea Conroy for their constructive comments on the manuscript. This work was supported by the Indiana University Health—Indiana University School of Medicine Strategic Research Initiative (N.W.S.), a grant from the National Institute of Allergy and Infectious Disease of the National Institutes of Health (R01 AI148525 to N.W.S.), and in part from federal funds from the National Institute of Allergy and Infectious Diseases, National Institutes of Health (U19AI110819 to H.L.). Support provided by the Herman B Wells Center was in part from the Riley Children's Foundation (N.W.S.). The Mali study was funded by the Division of Intramural Research, National Institute of Allergy and Infectious Diseases, National Institutes of Health. The content is solely the responsibility of the authors and does not necessarily represent the official views of the National Institutes of Health. This research was supported in part by Lilly Endowment, Inc., through its support for the Indiana University Pervasive Technology Institute. Sequencing analysis (shotgun metagenomics) was carried out in the Center for Medical Genomics at Indiana University School of Medicine, which is partially supported by the Indiana University Grand Challenges Precision Health Initiative.

Author contributions

K.V.M. contributed to the study concept and design, led the gnotobiotic mouse experiments and performed flow cytometry to measure parasitemia, prepared mouse and human fecal samples for subsequent sequencing and metabolomics measurements, performed quality control and taxonomic classification of sequencing data, analyzed and interpreted the data, and prepared the manuscript and figures. L.K.B. assisted with gnotobiotic mouse experiments. S.L. led sample management for the clinical study. H.L. prepared human fecal samples for 16S rRNA sequencing. S.D., D.D., K.K., A.O., and B.T. conceived the clinical study, participated in its design, and managed the collection of clinical data and biospecimens. P.D.C. conceived the clinical study, participated in its design and coordination in Mali, and reviewed the manuscript. N.W.S. contributed to the study concept and design, oversaw the execution of the experiments and the analysis of the data, and edited the manuscript. All authors read and approved the final manuscript.

Competing interests

The authors declare no competing interests.

Additional information

Supplementary information The online version contains supplementary material available at https://doi.org/10.1038/s41467-024-52953-8.

Correspondence and requests for materials should be addressed to Nathan W. Schmidt.

Peer review information *Nature Communications* thanks the anonymous reviewers for their contribution to the peer review of this work. A peer review file is available.